Identification and characterization of T reg–like cells in zebrafish

Melissa Kasheta,[1]* Corrie A. Painter,[1]* Finola E. Moore,[2,3,4,5] Riadh Lobbardi,[2,3,4,5] Alysia Bryll,[1] Eli Freiman,[1] David Stachura,[6] Arlin B. Rogers,[7] Yariv Houvras,[8] David M. Langenau,[2,3,4,5] and Craig J. Ceol[1]

[1]Program in Molecular Medicine and Department of Molecular, Cell and Cancer Biology, University of Massachusetts Medical School, Worcester, MA
[2]Molecular Pathology Unit and [3]Center for Cancer Research, Massachusetts General Hospital, Charlestown, MA
[4]Center for Regenerative Medicine, Massachusetts General Hospital, Boston, MA
[5]Harvard Stem Cell Institute, Cambridge, MA
[6]Department of Biological Sciences, California State University, Chico, CA
[7]Department of Biomedical Sciences, Cummings School of Veterinary Medicine at Tufts University, North Grafton, MA
[8]Departments of Surgery and Medicine, Weill Cornell Medical College, New York, NY

Regulatory T (T reg) cells are a specialized sublineage of T lymphocytes that suppress autoreactive T cells. Functional studies of T reg cells in vitro have defined multiple suppression mechanisms, and studies of T reg–deficient humans and mice have made clear the important role that these cells play in preventing autoimmunity. However, many questions remain about how T reg cells act in vivo. Specifically, it is not clear which suppression mechanisms are most important, where T reg cells act, and how they get there. To begin to address these issues, we sought to identify T reg cells in zebrafish, a model system that provides unparalleled advantages in live-cell imaging and high-throughput genetic analyses. Using a *FOXP3* orthologue as a marker, we identified CD4-enriched, mature T lymphocytes with properties of T reg cells. Zebrafish mutant for *foxp3a* displayed excess T lymphocytes, splenomegaly, and a profound inflammatory phenotype that was suppressed by genetic ablation of lymphocytes. This study identifies T reg–like cells in zebrafish, providing both a model to study the normal functions of these cells in vivo and mutants to explore the consequences of their loss.

INTRODUCTION

Studies of hematopoiesis in the zebrafish have defined major blood lineages. In the kidney marrow, the site of adult hematopoiesis, erythroid, lymphoid, and myeloid cells are present and can be separated based on light-scattering characteristics (Traver et al., 2003). However, subsets of cells within each of these lineages are poorly defined, primarily because of the lack of markers to distinguish a desired subset from other cells within the same lineage. In the lymphoid lineage, *lck:EGFP* and *cd4-1:mCherry* transgenes (Langenau et al., 2004; Dee et al., 2016) have been used to isolate bulk and CD4+ T cells, respectively, but thus far no markers have been established to further separate T cell sublineages. Indeed, it is not clear which sublineages of hematopoietic cells are present in zebrafish. Defining these sublineages in the zebrafish would further enable studies of developmental hematopoiesis, hematologic disease, and evolutionary immunology.

Among T cell subsets, regulatory T (T reg) cells are distinguished by their immunosuppressive activities. They are particularly important in maintaining peripheral tolerance by suppressing autoreactive T cells that escape negative selection in the thymus or inactivation in the periphery. A defining characteristic of T reg cells is their expression of the *FOXP3* transcription factor. *FOXP3* regulates expression of a suite of target genes, some of which are important for establishing the T reg lineage and others that are key mediators of T cell activation (Marson et al., 2007; Zheng et al., 2007; Birzele et al., 2011). *FOXP3* function is required for T reg development, and its loss in humans and mice results in T reg deficiency, leading to severe congenital autoimmune reactivity and other immunopathologies (Bennett et al., 2001; Brunkow et al., 2001; Wildin et al., 2001). Depletion of T reg cells in adults likewise causes inappropriate immunoreactivity, which is characterized by severe lympho- and myeloproliferation accompanied by pervasive inflammation (Kim et al., 2007; Lahl et al., 2007).

Whereas in vitro studies have characterized the functional basis for T reg–mediated immune suppression, the mechanisms by which these cells exert their functions

---

in vivo are poorly understood. Multiple mechanisms for T reg activity have been defined—production of immunosuppressive cytokines, cytolysis of target cells, cytokine deprivation or metabolic disruption of target cells, modulation of dendritic cell activity—but the relative importance of each in a variety of T reg functions has yet to be determined. Furthermore, the anatomical locations in which T reg cells mediate suppression in trans are only beginning to be explored. Liu et al. (2015) used high-resolution, spatially reconstructed histology to show that colocalization of T reg cells and target autoreactive T cells in the gut is important for T reg–mediated suppression. Although some progress has been made, these studies have been hampered by the inability to live-image cells in their native environments. In some studies, T reg cells have been adoptively transferred into mice and their interactions tracked (Mempel et al., 2006; Bauer et al., 2014), but to date there has been no way of visualizing the trafficking of these cells and their associations in a native setting. In the zebrafish, labeling bulk T cells with *lck:EGFP* has been instrumental in determining the locations of developmental hematopoiesis as well as providing a means to monitor acute T cell lymphoblastic leukemia (T-ALL) progression (Langenau et al., 2004; Frazer et al., 2009). More recently, *cd4-1:mCherry* transgenic zebrafish have been used to visualize this subset of T cells. In this study, *cd4-1:mCherry*–positive T cells from several anatomical sites were analyzed, and up-regulation of *foxp3* expression was observed in cells from some tissues, suggesting that T reg–like cells might be present and enriched in certain tissues (Dee et al., 2016). Given the ability to directly visualize native cells in zebrafish, identification of T reg cells in zebrafish would provide a platform to further understand how these cells interact with other immune cells, traffic through tissues, and are recruited to cancers. Indeed, a preponderance of tumor-resident T reg cells is linked to cancer-driven immunosuppression and poor clinical outcomes (Roychoudhuri et al., 2015), and determining how these cells function in this milieu could further enhance the effectiveness of immune checkpoint therapies.

To address these issues, we sought to determine whether T reg cells were present in zebrafish. Using a *FOXP3* orthologue as a marker, we identified CD4-enriched, mature lymphocytes with several hallmarks of T reg cells. Animals mutant for this *FOXP3* orthologue display hematopoietic imbalances characterized by excess T lymphocytes. Furthermore, these mutants have a severe inflammatory defect that results from inappropriate lymphocyte activity. Together, these data indicate that T reg–like cells are present in zebrafish and are required for proper immunoregulation. The ability to isolate and modulate the function of T reg–like cells in zebrafish opens up new avenues for studying the normal regulation of immunity by T reg cells as well as the role of these cells in pathological conditions such as autoimmunity and cancer.

RESULTS AND DISCUSSION

Generation of a *foxp3a:EGFP* reporter line

T reg cells are characterized by specific expression of the *FOXP3* transcription factor. There are two *FOXP3* orthologues in zebrafish, *foxp3a* and *foxp3b*, each of which is similarly diverged from mammalian *FOXP3* (Fig. 1 A). To determine whether one or both of these could mark zebrafish T reg cells, if present, we performed quantitative RT-PCR (qRT-PCR) analysis of zebrafish whole kidney marrow (WKM), the site of hematopoiesis in adult zebrafish (Fig. 1 B). *foxp3a* was highly enriched in WKM, whereas *foxp3b* levels were only modestly higher in WKM compared with nonhematopoietic control fin tissue. For this reason, we constructed a *foxp3a* reporter construct that placed 2.4 kb of *foxp3a* promoter sequence upstream of the *EGFP* gene. Zebrafish embryos were injected with this construct, and a stable transgenic line was obtained.

Characterization of *foxp3a:EGFP*–expressing cells

We performed flow cytometry to determine cell subsets that express *foxp3a:EGFP*. Cells from WKM of *Tg(foxp3a:EGFP)* animals were first plotted according to side-scatter and EGFP positivity, then cells from the EGFP-positive population were plotted according to side- and forward-scatter (Fig. 1 C). Cells in the zebrafish WKM segregate into distinct blood populations based on light-scattering characteristics. Gates corresponding to erythroid, lymphoid, precursor, and myeloid-containing populations were assigned based on our own (Fig. S1 A) and previous (Traver et al., 2003; Lin et al., 2005) data. Most *foxp3a:EGFP*-positive cells were found in the lymphoid-containing gate. Using a different gating strategy, we examined whether *foxp3a:EGFP*-positive cells were present in other blood populations. We first plotted cells according to side- and forward-scatter, then from each blood population, we determined the percentage of cells that were EGFP-positive (Fig. 1 D and Fig. S1 A). The fraction of EGFP-positive cells in the lymphoid-containing gate represented a 132-fold increase in *Tg(foxp3a:EGFP)* animals compared with control animals. Nonlymphocytes that gated as EGFP-positive were present in wild-type AB animals; thus such cells in *Tg(foxp3a:EGFP)* animals were most likely background cells with intrinsic autofluorescence. To further investigate the nature of *foxp3a:EGFP*-positive cells from the lymphoid gate, we isolated these cells by FACS and viewed their morphology using May-Grünwald Giemsa staining. *foxp3a:EGFP*-positive cells had a lymphoid morphology similar to *lck:EGFP*-positive T lymphocytes (Fig. 1 E). *foxp3a:EGFP*-positive cells were also absent in *rag1(lf)* WKM (Fig. 1, D and F). Finally, we did not detect *foxp3b* expression in *foxp3a:EGFP*-positive cells or bulk lymphocytes, suggesting that *foxp3b* does not act redundantly with *foxp3a*, nor does it act in a separate, *foxp3a*-independent population of WKM lymphocytes (Fig. 1 G). Its expression in whole WKM could reflect its presence in WKM stromal cells or nonlymphocyte hematopoietic populations. The low level of *foxp3b* in WKM
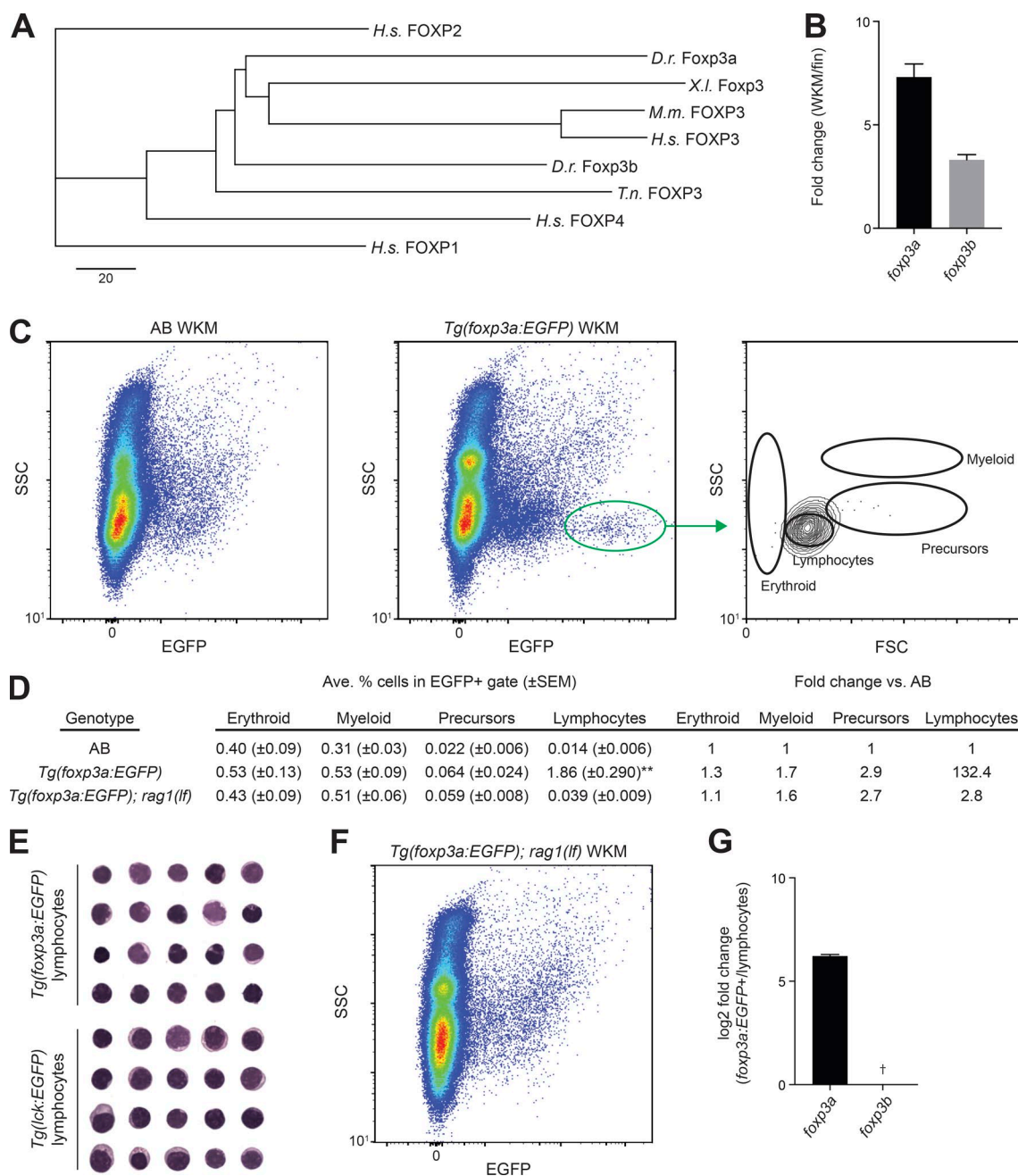
A

H.s. FOXP2
D.r. Foxp3a
X.l. Foxp3
M.m. FOXP3
H.s. FOXP3
D.r. Foxp3b
T.n. FOXP3
H.s. FOXP4
H.s. FOXP1

20

B

Fold change (WKM/fin)

foxp3a   foxp3b

C

AB WKM

Tg(foxp3a:EGFP) WKM

SSC — EGFP

Myeloid
Precursors
Lymphocytes
Erythroid

SSC — FSC

D

Genotype	Ave. % cells in EGFP+ gate (±SEM)				Fold change vs. AB			
	Erythroid	Myeloid	Precursors	Lymphocytes	Erythroid	Myeloid	Precursors	Lymphocytes
AB	0.40 (±0.09)	0.31 (±0.03)	0.022 (±0.006)	0.014 (±0.006)	1	1	1	1
Tg(foxp3a:EGFP)	0.53 (±0.13)	0.53 (±0.09)	0.064 (±0.024)	1.86 (±0.290)**	1.3	1.7	2.9	132.4
Tg(foxp3a:EGFP); rag1(lf)	0.43 (±0.09)	0.51 (±0.06)	0.059 (±0.008)	0.039 (±0.009)	1.1	1.6	2.7	2.8

E

Tg(foxp3a:EGFP) lymphocytes

Tg(lck:EGFP) lymphocytes

F

Tg(foxp3a:EGFP); rag1(lf) WKM

SSC — EGFP

G

log2 fold change (*foxp3a:EGFP+/lymphocytes*)

foxp3a   foxp3b †

Figure 1. **Foxp3 phylogeny and identification of *foxp3a:EGFP*–positive lymphocytes.** (A) Phylogenetic relationship of zebrafish Foxp3 proteins to Foxp3 proteins from other species (human, *Homo sapiens,* H.s.; mouse, *Mus musculus,* M.m.; frog, *Xenopus laevis,* X.l.; pufferfish, *Tetraodon nigroviridis,* T.n.) and other human Foxp family proteins. Unrooted neighbor-joining best trees were produced using MacVector v12.5.1. Sequences were aligned by ClustalW. Distance was absolute, and gaps were distributed proportionally. GenBank accession nos. for sequences used were D.r. Foxp3a (NP_001316496), D.r. Foxp3b (XM_021478427), H.s. Foxp1 (NP_001231745), H.s. Foxp2 (NP_055306), H.s. Foxp3 (ABQ15210), H.s. Foxp4 (NP_001012426), M.m. Foxp3 (NP_001186277), X.l. Foxp3 (NP_001121199), and T.n. Foxp3 (ADD91631). (B) qRT-PCR of *foxp3* paralogs in wild-type AB WKM relative to nonhematopoietic fin tissue. Error bars indicate SEM; $n = 3$. (C) Flow cytometry analysis of WKM from representative AB and *Tg(foxp3a:EGFP)* animals. Gates of major hematopoietic lineages are indicated at right. (D) Percentages of *EGFP*-positive cells in each gate are shown, and data were used to calculate fold differences of *EGFP*-positive cells in *Tg(foxp3a:EGFP)*; $n = 5$) and *Tg(foxp3a:EGFP); rag1(lf)* ($n = 5$) versus intrinsically fluorescent cells in wild-type AB animals ($n = 5$). Two-tailed Student's *t* test, *Tg(foxp3a:EGFP)* versus *Tg(foxp3a:EGFP); rag1(lf)*, **, P < 0.001. (E) Cytological stains of sorted *foxp3a:EGFP*-positive cells compared with sorted *lck:EGFP*-positive lymphocytes. Individual cells were extracted and aligned for comparative purposes. (F) Flow cytometry of WKM from a representative *Tg(foxp3a:EGFP); rag1(lf)* animal showing absence of the *EGFP*-positive population. (G) qRT-PCR of *foxp3* paralogs in *foxp3a:EGFP*-positive cells from WKM compared with bulk WKM lymphocytes. †, Expression of *foxp3b* was below the limit of detection in *foxp3a:EGFP*-positive and bulk lymphocytes. Error bar indicates SEM; $n = 3$.
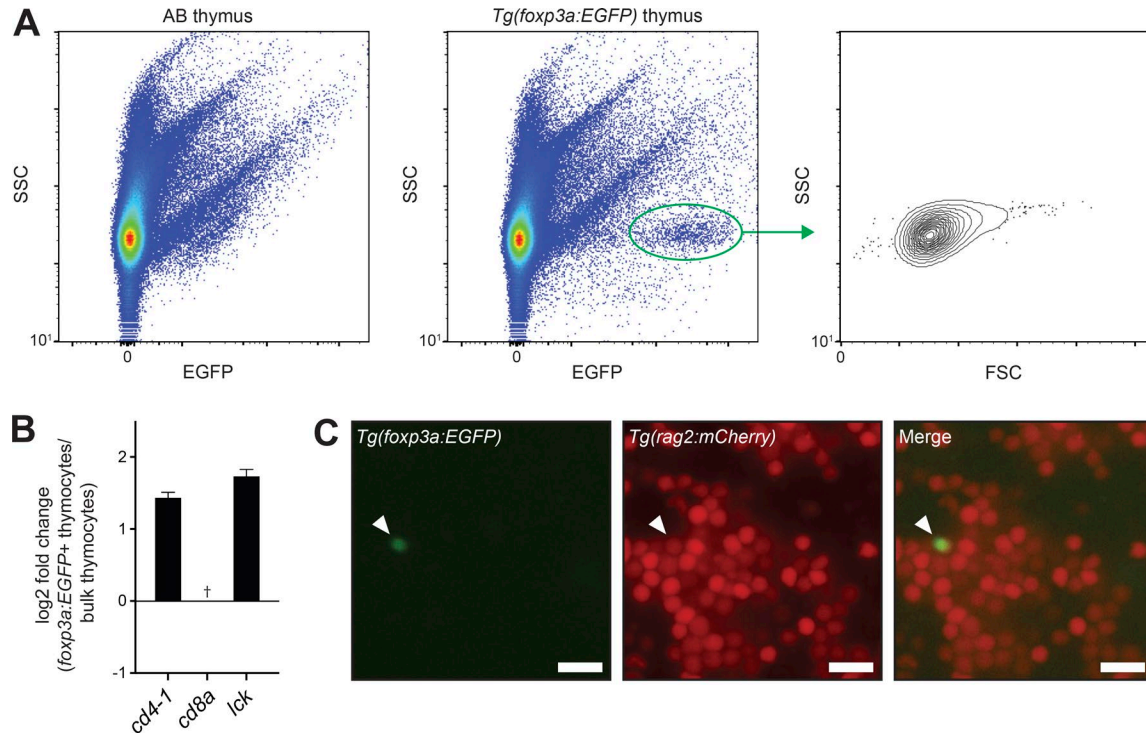
Figure 2. Identification and analysis of *foxp3a:EGFP*–positive thymocytes. (A) Flow cytometry analysis of thymus from representative AB and *Tg(foxp3a:EGFP)* animals. (B) qRT-PCR of selected genes in *foxp3a:EGFP*-positive thymocytes relative to bulk thymocytes. Relative CD4 and CD8 expression is also shown and represents zebrafish *cd4-1* and *cd8a* genes. †, Expression of *cd8a* was below the limit of detection in *foxp3a:EGFP*-positive thymocytes. Error bars indicate SEM.; *n* = 3. (C) Cells from dissected thymus of a *Tg(foxp3a:EGFP); Tg(rag2:mCherry)* animal showing a double-positive thymocyte (arrowheads). Bars, 10 µm.

also does not exclude the possibility that it is expressed in lymphocytes present in other tissues. Collectively, based on light-scattering characteristics, cellular morphology, and requirement for *rag1*, *foxp3a:EGFP* cells are lymphocytes.

We looked for *foxp3a:EGFP* cells in other tissues. We assessed thymocytes from *Tg(foxp3a:EGFP)* animals using flow cytometry. In whole-thymus preparations, an EGFP-positive population that mapped to the lymphocyte gate was evident in *Tg(foxp3a:EGFP)* animals (Fig. 2 A). These *foxp3a:EGFP*-positive thymocytes had higher expression of the *CD4* orthologue *cd4-1* compared with bulk thymocytes, whereas expression of the *CD8* orthologue *cd8a* (Fig. 2 B) was not detected. The regulator of T cell activation *lck* was expressed in the *foxp3a:EGFP* population. We also examined thymocytes from *Tg(rag2:mCherry); Tg(foxp3a:EGFP)* animals. Of explanted *rag2:mCherry*-positive thymocytes, rare cells were also *foxp3a:EGFP*-positive (Fig. 2 C). Because *foxp3a*-positive thymocytes were present in zebrafish, we speculate that development of some *foxp3a*-positive cells occurs in the thymus. In surveying other anatomical sites, we found that *foxp3a:EGFP*-positive cells were present in the skin. By flow cytometry, a population of EGFP-positive cells with characteristics of lymphocytes was evident (Fig. S1 B). Compared with bulk skin lymphocytes, these cells expressed higher levels of *cd4-1*, and *cd8a* expression was not detected (Fig. S1 C). We were unable to detect *lck* expression in this subpopulation. It is known that human skin-resident T reg cells express lower levels of *LCK* (Ali et al., 2017), although whether this lower expression reflects a functional difference in this subpopulation has not been investigated. We tracked the motility of *foxp3:EGFP*-positive cells in the skin with live-cell, time-lapse imaging (Fig. S1 D and Video 1). Directional motility of these cells was characterized by the formation of extensions at the leading edge of the cell followed by migration of the cell body. *foxp3a:EGFP* cells were highly motile in the skin, which may be evidence of their surveillance of this tissue. Finally, intermyseal connective tissue boundaries between muscle segments contained *foxp3a: EGFP*-positive cells (Fig. S1 E). In mammals, the thymus, skin, and muscle each contain *FOXP3*-expressing T reg cells (Panduro et al., 2016).

Gene expression in *foxp3a:EGFP*–positive cells

We characterized gene expression in *foxp3a:EGFP*-positive cells. For transcriptome analyses, EGFP-positive lymphocytes were harvested from the WKM of *Tg(foxp3a:EGFP)* and *Tg(lck: EGFP)* animals and used for low-input RNA extraction and library preparation followed by massively parallel sequencing
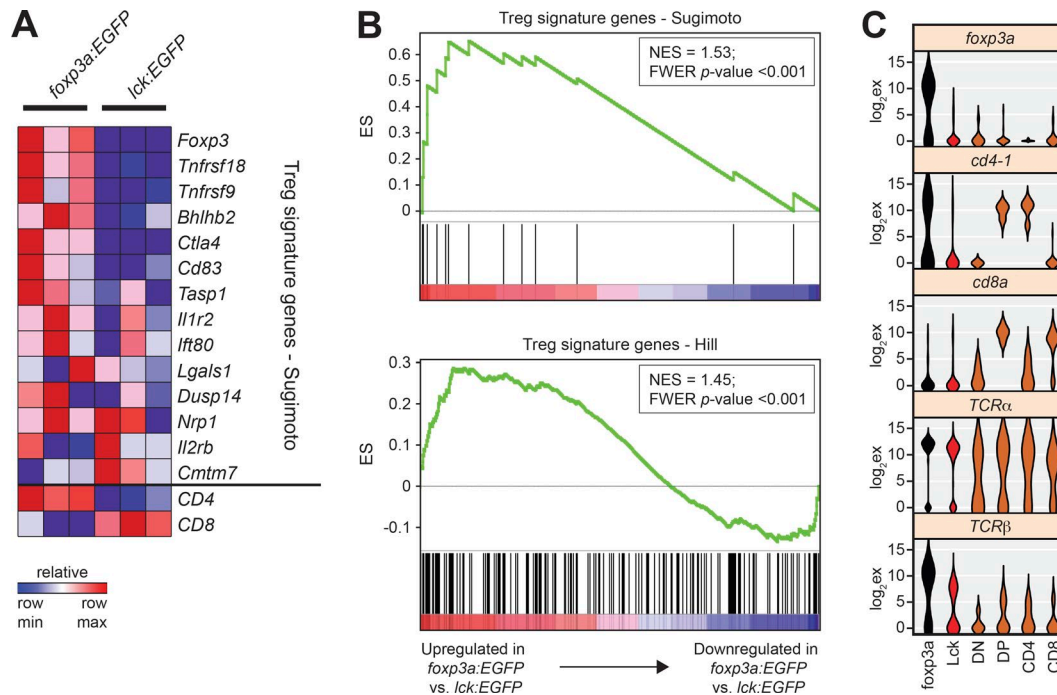
Figure 3. Expression analyses of *foxp3a:EGFP*–positive cells. (A) Heat map of T reg signature genes as defined by Sugimoto et al. (2006). Mouse gene names are indicated. Only genes with a normalized read count >10 are shown, as are genes with unambiguous zebrafish-to-mouse orthology, except for *Foxp3*, for which expression values of *foxp3a* are represented. (B) Top, GSEA showing that expression of a T reg signature, as defined by Sugimoto et al. (2006), is enriched in zebrafish *foxp3a:EGFP* cells. Bottom, GSEA showing enrichment of a broader T reg signature, as defined by Hill et al. (2007). (C) Violin plots from single-cell analyses showing that the expression profile of *foxp3a:EGFP*–positive cells is biased to that of mature (TCR$^+$) *cd4-1$^+$cd8a$^-$* lymphocytes. Cell populations were assigned from single-cell analyses of sorted *lck:EGFP*-positive (Lck) and thymic (double-negative [DN], double-positive [DP], CD4, and CD8) cells. By ANOVA, *foxp3a* (P = 1.61 × 10^{-22}), *cd4-1* (P = 1.02 × 10^{-36}), *cd8a* (P = 1.35 × 10^{-58}), *TCR*α (P = 2.60 × 10^{-6}), and *TCR*β (P = 5.18 × 10^{-8}).

(RNA-seq). Zebrafish genes with orthology to murine genes were used to compare expression profiles of *foxp3a:EGFP*-positive cells to mammalian T reg cells. Zebrafish orthologues were first compared with a narrowly defined T reg signature (Sugimoto et al., 2006). Many of these zebrafish orthologues were up-regulated in *foxp3a:EGFP*-positive cells compared with *lck:EGFP*-positive T cells (Fig. 3 A). Gene set enrichment analysis (GSEA) confirmed that there is a significant correlation between this T reg signature and zebrafish orthologues up-regulated in *foxp3a:EGFP*-positive cells (Fig. 3 B). GSEA also revealed that another, more broadly defined murine T reg signature (Hill et al., 2007) was enriched in *foxp3a:EGFP*-positive cells (Fig. 3 B). Relative expression levels of a subset of deregulated genes were confirmed using qRT-PCR (Fig. S2 A). These analyses indicate that *foxp3a:EGFP* cells have a gene expression signature that is consistent with expression signatures found in T reg cells. In light of these similarities, we are referring to *foxp3a*-positive cells in zebrafish as T reg–like cells.

We performed single-cell analyses to examine gene expression profiles and heterogeneity of *foxp3a:EGFP*-positive cells. *foxp3a:EGFP*-positive cells from WKM were isolated using FACS, and single cells were arrayed for qRT-PCR. qRT-PCR measured levels of 96 genes, which comprise mostly markers of different blood cell lineages as well as some housekeeping genes (Moore et al., 2016a). Using these expression data, unsupervised hierarchical clustering was performed to compare *foxp3a:EGFP*-positive cells (n = 35 cells) with unselected WKM cells from wild-type AB animals (n = 85 cells; Fig. S2 B). WKM cells fall into four distinct gene expression clusters, which correspond to T and B lymphocytes and erythroid and myeloid cells. Thirty *foxp3a:EGFP*-positive cells clustered with T lymphocytes. In considering individual genes (Fig. 3 C and Fig. S2 B), most cells (30/35) expressed T cell receptor genes. The largest fraction of cells (17/35) were *cd4-1$^+$cd8a$^-$*. Two cells were *cd4-1$^-$cd8a$^+$*. Several cells (11/35) were TCR–positive but *cd4-1$^-$cd8a$^-$*. Because extrathymic double-negative cells are rare and do not express FOXP3 (Hillhouse and Lesage, 2013), it is suspected that at least some of these cells express a second CD4 homologue, *cd4-2*, that is expressed in zebrafish lymphocytes (Yoon et al., 2015) but was not present in the single-cell analysis pipeline. *cd4-2* was expressed in the *foxp3a:EGFP*-positive population at higher levels than in *lck:EGFP*-positive lymphocytes (Fig. S2 A). In addition to *foxp3a:EGFP*-positive cells that clustered with lymphocytes, there were five cells that segregated to the erythroid cluster. One of these cells expressed several red cell markers, and the four others were "low-expressor" cells that

A

```
WT     CCTGGAGACAGAAGCATAGGCCAGCTGAGGATGCAGAAAGACAGAGTACAGCA
um252  CCTGGAGACAGAAGCAT-------CTG----TGCAGAAAGACAGAGTACAGCA
um253  CCTGGAGACAGAA--------------AGGATGCAGAAAGACAGAGTACAGCA
```
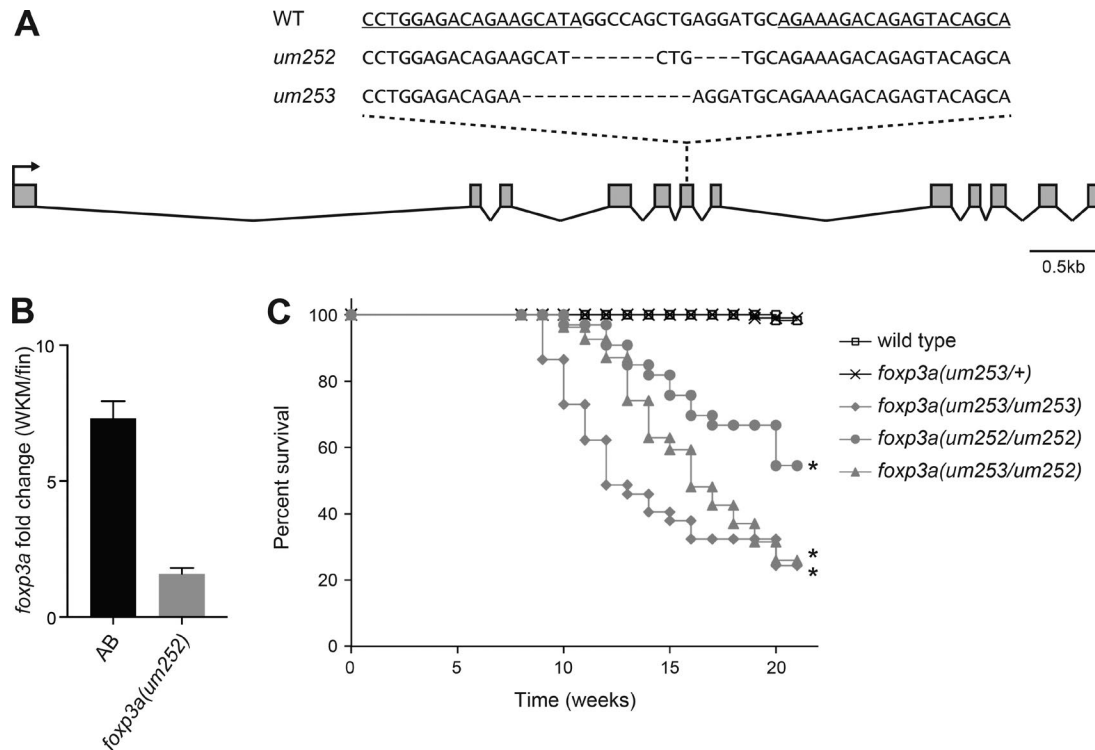
0.5kb

B

C

Figure 4. **foxp3a mutations and effects on survival.** (A) Gene structure of *foxp3a* with sites and sequences of mutations indicated. (B) qRT-PCR of *foxp3a* in WKM relative to nonhematopoietic fin tissue. *foxp3a(um252)* animals show a reduction of *foxp3a* transcripts. Error bars indicate SEM; n = 3. (C) Kaplan–Meier survival analysis of *foxp3a* mutants compared with wild-type animals. Log-rank (Mantel–Cox) test, *, P < 0.0001 for pairwise comparisons of *foxp3a(um252/um252)* (n = 37), *foxp3a(um253/um253)* (n = 33), and *foxp3a(um252/um253)* (n = 54) versus wild type (n = 59).

showed undetectable expression of most genes. Additional markers would be required to determine whether such cells represent distinct subpopulations of *foxp3a:EGFP*-positive cells. Overall, a comparison of gene expression to that in other T cell subsets indicates that most *foxp3a:EGFP*-positive cells are mature T cells with a bias toward CD4 positivity (Fig. 3 C). However, single-cell analyses reveal that there is some heterogeneity in the *foxp3a:EGFP*-positive population.

Identification of *foxp3a* mutants

Mutations in mammalian *FOXP3* genes cause loss of T reg cells, resulting in IPEX (immunodysregulation polyendocrin-opathy enteropathy X-linked) syndrome in humans and the Scurfy phenotype in mice, both of which are characterized by an inflammatory response as a result of severe autoimmunity. To determine the consequences of *foxp3a* loss in zebrafish, we used site-directed transcription activator-like effector nucleases (TALENs) to induce *foxp3a* mutations. A region before the coding sequence for the *foxp3a* DNA-binding domain, in the sixth exon, was targeted. We injected TALEN mRNAs targeting this region into zebrafish embryos, allowed these animals to mature, then screened their progeny for *foxp3a* mutations. Animals with two independently derived mutations were recovered. The mutations, *um252* and *um253*, created small deletions in the *foxp3a* gene and, by

removing 11 and 14 nt, respectively, are predicted to cause premature truncations of the Foxp3a protein (Fig. 4 A). We performed qRT-PCR to measure RNA transcript levels in the WKM of *foxp3a(um252)* mutants and found that *foxp3a* transcripts were substantially reduced, presumably because of nonsense-mediated decay (Fig. 4 B).

We created a strain that combined the *Tg(foxp3a: EGFP)* transgene with the *foxp3a(um252)* mutation to determine whether T reg–like cells were affected by loss of *foxp3a* function. Flow cytometry of WKM from these animals showed, surprisingly, that there was an expansion of *foxp3a: EGFP*-positive cells (Fig. S3, A and B). To assess the nature of these cells, we isolated them using FACS and performed qRT-PCR (Fig. S3 C). As expected, the level of endogenous *foxp3a* transcripts in these cells was reduced. Normal *foxp3a: EGFP*-positive cells have low levels of *cd8a*; however, mutant *foxp3a:EGFP*-positive cells showed substantial expression of *cd8a*. Furthermore, expression of orthologues of mammalian T reg–enriched genes was deregulated in mutant *foxp3a:EGFP*-positive cells compared with their normal counterparts. *foxp3b* expression was not detected in mutant *foxp3a:EGFP*-positive cells, suggesting that it likely is not up-regulated to compensate for the loss of *foxp3a*. Based on these results, *foxp3a: EGFP*-positive cells from *foxp3a* mutants have an expression profile that is different from that of wild-type *foxp3a:EGFP*-

positive cells. In some *FOXP3* mutant IPEX patients, expanded populations of *FOXP3*-expressing cells have been observed, but these cells are similarly deranged in their misexpression of CD8 and other sublineage markers (Gavin et al., 2006). Furthermore, cells expressing a *Foxp3:EGFP* transgene are present in *Foxp3* mutant mice, and these cells also misexpress CD8 and other T reg signature genes (Lin et al., 2007). As has been suggested in these mammalian cases, we speculate that presumptive T reg–like cells develop in *foxp3a* mutants but encounter a differentiation block in the absence of *foxp3a* function and ultimately adopt a hybrid profile with concurrent *foxp3a* promoter activity and *cd8a* expression.

Poor survival of *foxp3a* mutant strains

The survival of *foxp3a* mutants was measured with cohorts of *foxp3a* heterozygous and homozygous mutant animals. After 20 wk, all control animals remained alive, whereas profound reductions in survival were observed in *foxp3a(um252)* and *foxp3a(um253)* homozygotes (Fig. 4 C). Reduced survival was also found in *foxp3a(um252/um253)* mutants, indicating that this survival defect was likely caused by loss of *foxp3a* function rather than background mutations present in the independently isolated *foxp3a* mutant strains. Aside from moderate wasting, no outwardly visible defects were present in *foxp3a* mutants before death.

Hematopoietic defects in *foxp3a* mutants

foxp3a mutants were analyzed for hematopoietic defects. By flow cytometry, differences between control *foxp3a* heterozygous animals and *foxp3a* homozygous mutants were apparent (Fig. 5 A). Most noticeable was the increase of cells in the lymphoid-containing gate present in WKM from *foxp3a(um252)* and *foxp3a(um253)* mutants. Again, because similar hematopoietic defects were observed in *foxp3a (um252/um253)* mutants, this abnormality is likely caused by loss of *foxp3a* function. To better quantify differences in cell numbers, May-Grünwald Giemsa staining was performed on WKM, and nonerythroid cells were counted (Fig. 5 B). Lymphocytes were indeed increased, and a commensurate decrease in myeloid cells was observed. Inappropriate expansion of lymphocytes occurs in IPEX patients and Scurfy mice as a result of loss of T reg–mediated immune suppression. *foxp3a* mutants show a similar lymphocyte expansion.

foxp3a deficiency results in splenomegaly and chronic inflammation

We sacrificed and sectioned *foxp3a* mutants to assess whether additional internal defects could be compromising the health of these animals. Despite being smaller in overall size (Fig. S3 D), *foxp3a* mutants displayed marked splenomegaly (Fig. 5 C and Fig. S3 E). Visual examination of dissected spleens from *foxp3(um252); Tg(lck:EGFP)* animals suggested that this splenomegaly was characterized by an increased content of T lymphocytes (Fig. 5 D). Quantification of splenic *lck:EGFP*-positive cells from these animals confirmed this:

although somewhat variable, spleens from *foxp3a* mutants contained a mean fourfold increase in T lymphocytes (Fig. 5 E and Fig. S3, F and G).

Pathological examination revealed profound inflammation of coelomic connective tissue surrounding the terminal colon and urogenital pore (Fig. 5 F). Inflammation extended into the ventral skin surrounding this pore (Fig. 5 G). In this and other inflamed regions, a lymphocyte–predominant mononuclear cell inflammatory infiltrate was present at much higher levels than in the same regions of control animals. In IPEX syndromic patients and Scurfy mice, persistent inflammation is present in multiple tissues and is driven by overexuberant cytokine production by and reactivity of lymphocytes. Inflammation in *foxp3a* mutant fish also likely results from aberrant lymphocytic reactivity, as *foxp3a(um252); rag1(lf)* fish have no inflammatory phenotype (Fig. 5, F and G). To assess whether an enhanced inflammatory response was associated with death of *foxp3a* mutants, we examined expression of inflammation marker genes in moribund *foxp3a* mutant and wild-type AB animals. In both colon and skin samples from *foxp3a(um252)* mutants, we observed an elevated level of the IFN-γ gene *ifng1-2*, as indicated by lower ΔCt values (Fig. 5 H). Levels of an interleukin-1β orthologue, *il1b*, were also elevated in colon samples of *foxp3a(um252)* mutants. *il1b* levels in skin were not significantly altered, nor were levels of a TNF-α homologue, *tnfa*, in skin or colon (Fig. S3 H). Based on these results, aspects of a pathological and molecular inflammatory response were associated with the death of *foxp3a* mutant animals.

In mammals, T reg cells play an essential role in suppressing autoreactive T cells. The adaptive immune system arose ~500 million years ago in jawed fish (Flajnik and Kasahara, 2010), but it has not been clear whether mechanisms to curtail autoimmunity were present in the earliest adaptive immune systems. Arguing against the possibility of ancestral T reg cells, comparative analyses of FOXP3 orthologues showed that nonmammalian FOXP3 genes lack structural domains necessary for specification of the T reg sublineage (Andersen et al., 2012). However, our identification of T reg–like cells in zebrafish suggests that these cells were present at or near the emergence of adaptive immunity. In zebrafish, expression of *cd4-1* is enriched in T reg–like cells, and these cells share a gene expression profile similar to that of mammalian T reg cells. Although an in vitro assessment of T reg suppression activity is currently not possible (appropriate cytokines have not yet been isolated), in vivo analyses of *foxp3a* mutants strongly suggest that zebrafish T reg–like cells have suppressor activity. The features of zebrafish T reg–like cells, along with the finding of *foxp3*-expressing blood cells in the pufferfish (Wen et al., 2011), suggest that T reg cells were an early sublineage of the adaptive immune system.

Because T reg–like cells are present in the zebrafish, the unique attributes of this model system can be harnessed to study this cell type. Ex vivo development of zebrafish embryos
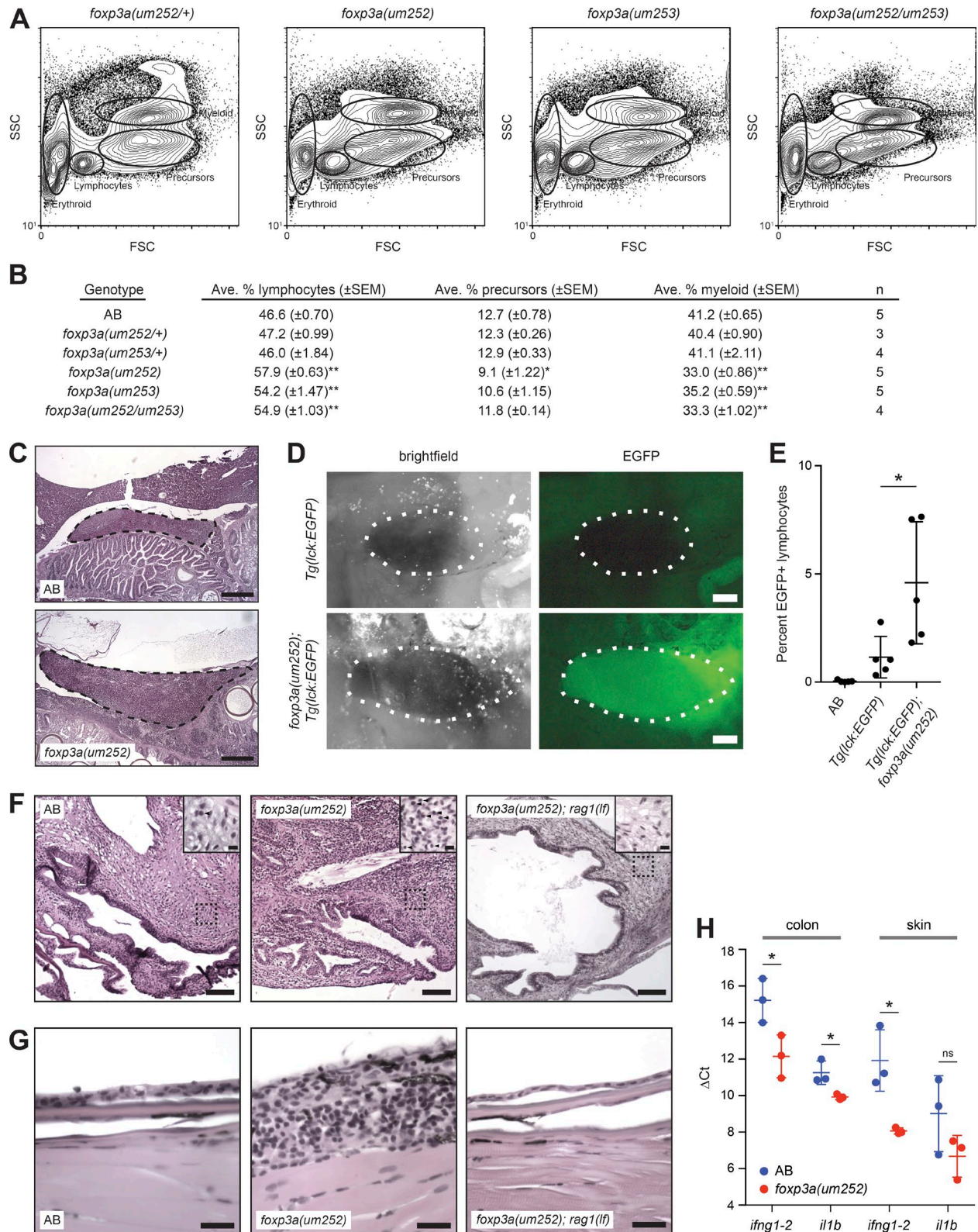
Figure 5. **Lymphocyte expansion and lymphocyte–dependent inflammation in *foxp3a* mutants.** (A) Flow cytometry analyses of WKM from representative *foxp3a* mutant animals. (B) Differential counts of nonerythroid cells from WKM. Counts were obtained from at least 200 cells per WKM cytospin with May-Grünwald Giemsa staining. Two-tailed Student's *t* test (*foxp3a* mutant vs. AB), *, P < 0.05; **, P < 0.001. (C) Representative images of hematoxylin and eosin–stained sagittal sections of spleens from wild-type AB and *foxp3a(um252)* mutants. Images showing largest extent of splenic size

has facilitated studies of developmental hematopoiesis (Robertson et al., 2016), and through similar analyses, the developmental lineage and molecular specification of T reg–like cells can be examined. We have shown that direct imaging of T reg–like *foxp3a:EGFP*-positive cells can be performed. These cells are highly motile as they traffic through tissues. Through the combined use of the *foxp3a:EGFP* reporter and reporters of other cell types, it will be possible to visualize interactions of T reg–like cells with target T cells and other types of blood cells. In addition, implementation of zebrafish cancer models will enable the study of these cells in a native tumor setting. Such studies will serve as an important complement to T reg cell interaction studies that are currently performed through intravital imaging of xenografted cells in mammalian systems (Bauer et al., 2014).

Mammalian T reg cells can either develop in the thymus or differentiate without thymic education in the periphery. Development of thymic T reg cells is promoted by high-affinity interactions with self-peptide–MHC complexes, whereas peripheral T reg cells are thought to differentiate in response to non–self antigens, including allergens and commensal microbiota (Josefowicz et al., 2012). We found that a subset of thymocytes express *foxp3a*, suggesting that at least some T reg–like cells develop in the thymus and may be involved in suppressing autoimmunity. In human IPEX patients and Scurfy mice, autoimmunity caused by lack of T reg cells results in a gross inflammatory phenotype that is associated with excess lymphocyte activity (Lyon et al., 1990; Wildin et al., 2002). In addition, the expansion of T lymphocytes and splenomegaly are observed in *FOXP3*-deficient mammals (Powell et al., 1982; Kim et al., 2007). Altogether, *foxp3a* mutant zebrafish have a similar constellation of defects as, and can thus serve as a suitable model for, *FOXP3*-deficient mammals.

Although the existence of T reg cells was established nearly two decades ago, several important issues regarding their functions remain to be elucidated. In particular, the mechanisms by which they dominantly suppress immune responses in vivo, the sites at which they interact with target cells, and their involvement in pathological conditions such as tumor immune suppression are all poorly understood. Through the identification of zebrafish T reg–like cells and the development of *foxp3a*-deficient mutants, many of these issues can be addressed.

MATERIALS AND METHODS

Strains
Zebrafish were maintained at 28.5°C with a 14:10-h day:night cycle. *Tg(lck:EGFP)* (Langenau et al., 2004), *rag1(hu1999)* (Wienholds et al., 2002) strains were used. *rag1(hu1999)* mutants were provided by L. Petrie-Hanson (Mississippi State University, Starkville, MS). AB was used as the wild-type strain. All zebrafish studies were performed according to Institutional Animal Care and Use Committee guidelines and University of Massachusetts Medical School Animal Care Committee protocols.

Generation of *foxp3a:EGFP* transgenic line
A gene structure for *foxp3a* was determined based on available cDNA sequences. A 2,446-bp promoter fragment upstream of the 5′-most noncoding exon was PCR-amplified (corresponding to −7,448 to −5,003 relative to the *foxp3a* initiator ATG) and recombined into the Gateway P4P1r vector (Thermo Fisher Scientific). Using multisite Gateway recombination, the *foxp3a* promoter was placed upstream of the *EGFP* gene followed by an SV40 polyadenylation signal in the pDestTol2CG2 vector (Kwan et al., 2007). Single-cell embryos were injected and transgenic founders selected based on heart fluorescence.

cDNA synthesis and qRT-PCR
Total RNA was isolated from WKM and sorted cells using TRIzol-chloroform (Thermo Fisher Scientific) extraction followed by RNA cleanup (QIAGEN RNeasy). RNA was amplified and reverse-transcribed using the Ovation Pico WTA System v2 (NuGen). qRT-PCR was performed with SYBR green master mix (Applied Biosystems) using the following primers: *foxp3a*: forward, 5′-TGCTTTGTG CGTGTTGAAGG-3′, and reverse 5′-ACAGCTGAA ATGGTGCCATC-3′; *foxp3b*: forward, 5′-TTTAAAGCA GCACGCTTCAG-3′, and reverse, 5′-AGAAACTGCATT CGCTGCTC-3′; *cd4-1*: forward, 5′-TCAACACCAAGA CCATCAGC-3′, and reverse, 5′-GCACATGTCCATTTC ACCTC-3′; *cd4-2*: forward, 5′-TTATTCCTGCGCACA GTCAG-3′, and reverse, 5′-TTGGGCCTGGTTTAG CAAAC-3′; *cd8a*: forward, 5′-TCGGAGGTTGTGGAC TTTTC-3′, and reverse, 5′-TTGTAATGGTGGGGACAT CG-3′; *ctla4*: forward, 5′-GGGAACGGCACTGTTGTT TAC-3′, and reverse, 5′-TGTCTGGCTCTTGCTTTG

are shown. Spleens are shown bordered by dashed lines. Bars, 250 µm. (D) Representative images of dissected spleens from *Tg(lck:EGFP)* and *Tg(lck:EGFP); foxp3a(um252)* animals. Spleens are shown bordered by dotted lines. Bars, 250 µm. (E) Flow cytometry analysis of spleens from AB (*n* = 5), *Tg(lck:EGFP)* (*n* = 5) and *Tg(lck:EGFP); foxp3a(um252)* (*n* = 5) animals. Percentages of *EGFP*-positive cells in the lymphocyte gate are shown. Two-tailed Student's *t* test, *, P < 0.05. (F) Representative images of hematoxylin and eosin–stained sagittal sections of urogenital pores from wild-type AB, *foxp3a(um252)*, and *foxp3a(um252); rag1(lf)* animals. In total, 0/4 wild-type AB, 6/6 *foxp3a(um252)*, and 0/3 *foxp3a(um252); rag1(lf)* animals displayed connective tissue inflammation. Insets, increased cellularity characterized by marked influx of lymphocyte-predominant inflammatory cells (arrowheads) in *foxp3a(um252)* mutants compared with the wild-type AB and *foxp3a(um252); rag1(lf)* double mutants. Bars: 100 µm; (inset) 10 µm. (G) Representative images of hematoxylin and eosin–stained sagittal sections of skin from wild-type AB, *foxp3a(um252)*, and *foxp3a(um252); rag1(lf)* animals. In total, 0/4 wild-type AB, 5/6 *foxp3a(um252)*, and 0/3 *foxp3a(um252); rag1(lf)* animals displayed skin inflammation. Bar, 25 µm. (H) qRT-PCR analysis of inflammation marker genes *ifng1-2* and *il1b*. ΔCt values were calculated relative to a *β-actin* control. Two-tailed Student's *t* test, *, P < 0.05; ns, not significant. Error bar indicates SEM; *n* = 3.

AC-3′; *tnfrsf18*: forward, 5′-AACGATGTTGAGGACAGC
AC-3′, and reverse, 5′-TGCATTGTGGGTCTGGTTTC-
3′; *ikzf4*: forward, 5′-ATTGCAATGGCCGTTCGTAC-3′
and reverse, 5′-ATGGAGTTAGCACTGAGTGAGC-3′;
irf4b: forward, 5′-AACTGCAAACTGCTGGACAC-3′, and
reverse, 5′-ACAGCAACACTTGGGAACAC-3′; and *lck*:
forward, 5′-AGTGGCCCAGCATTGATATCTG-3′, and
reverse, 5′-ATCAAAAGAGCCGCAGTTCC-3′. Data from
three technical replicates per sample were obtained. In single-
cell analyses, cells were arrayed, RNA was extracted, and qRT-
PCR was performed using the Fluidigm BioMark HD as
described (Moore et al., 2016a,b). The panel of genes profiled
was described previously (Moore et al., 2016a). Ct values were
recovered from the BioMark HD. The quality threshold was set
to 0.65, and a linear derivative as baseline correction was used.
Using SINGuLAR software (Fluidigm), the limit of detection
was set to a Ct of 28; expression was calculated using default
settings. Sample wells that failed to express housekeeping
genes (*eef1a1l1* and *actb1*) or other lineage-specific markers
were deemed to lack a cell and were eliminated from further
analysis. Unsupervised hierarchical clustering was performed
using SINGuLAR. *foxp3a:EGFP*-positive single-cell samples
were combined and compared with the datasets generated
previously (Moore et al., 2016a), and lineage assignments were
made after hierarchical clustering. The hierarchical clustering
and violin plots were also generated using the SINGuLAR R
package, with the limit of detection set to a Ct of 28.

RNA–seq

EGFP-positive lymphocytes were sorted from the WKM of
Tg(foxp3a:EGFP) and *Tg(lck:EGFP)* animals to prepare three
biological replicate samples of each genotype. Sorted cells were
used to prepare amplified double-stranded (ds)-cDNA using
Clontech SMART-Seq v4 ultra low input RNA kit, according
to the manufacturer's recommendations. Amplified ds-cDNA
was purified, fragmented, and used to prepare libraries using
TruSeq RNA sample preparation kit v2 (Illumina). After
validation using a DNA 1000 LabChip (Agilent), samples were
submitted for RNA-seq. As described previously (Anelli et al.,
2017), paired end reads were aligned using Star v2.3 (Dobin et
al., 2013) to the zebrafish genome (GRCz10; Howe et al., 2013)
using the Ensembl transcriptome. Analysis of differential gene
expression was performed using DESeq2 (Love et al., 2014).
Orthology to murine genes was determined using Ensembl.

GSEA

For GSEA (Subramanian et al., 2005), a rank-ordered gene
list was made with normalized FPKM values from *foxp3a:
EGFP*-expressing cells compared with *lck:EGFP*-expressing
cells. Default parameters of GSEA were used, and Student's *t*
test was used to calculate significance.

Generation of *foxp3a* mutant strains

TALENs targeting the *foxp3a* locus were designed using the
TAL Effector Nucleotide Targeter 2.0. TALEs targeting the
sixth coding exon of the *foxp3a* gene (binding sites in caps,
spacer in lowercase: 5′-CCTGGAGACAGAAGCATAggc-
cagctgaggatgcAGAAAGACAGAGTACAGC-3′) were con-
structed using the GoldenGate TALEN and TAL Effector kit
2.0 (Addgene). RNA encoding *foxp3a*-directed TALENs was
injected into single-cell AB embryos, and progeny of injected
animals were screened for mutations. F1 progeny containing
foxp3a mutations were outcrossed to AB animals, and strains
were established. Mutant *foxp3a* alleles were detected by
PCR-amplifying an amplicon containing the TALEN target
site (forward primer, 5′-TGATTGGGTTGTGGACACC-3′;
reverse primer, 5′-CAGTTCTGAAGGCAAAGGG-3′) and
digesting with PvuII. Wild-type alleles are cut with PvuII,
whereas mutant alleles lack the PvuII site.

Flow cytometry and cell sorting

WKMs were harvested and prepared as previously described
(Traver et al., 2003), followed by flow cytometry using a FAC
SAriaII instrument (BD Biosciences). Spleens were harvested,
triturated, and subjected to the same preparation and flow
cytometry analysis as WKMs. FACS of WKMs was performed
using a FACSVantage instrument (BD Biosciences). Flow cy-
tometry data were analyzed using FlowJo software. Single
cells were sorted into 96-well plates using a FACSAria Fusion
Cell Sorter (BD Biosciences).

Cytology and histopathology

Cytospins were performed by applying 150 μl WKM cell
suspension to funnels and centrifuging for 5 min at 800 *g*.
Slides with cells were dried for 10–15 min. Stainings with
May-Grünwald and Giemsa solutions were performed as de-
scribed (Traver et al., 2003). For histopathology, humanely
euthanized fish were fixed whole in 10% neutral-buffered
formalin, sectioned sagittally, and routinely processed into
paraffin blocks. Hematoxylin and eosin–stained sections were
reviewed by A.B. Rogers, who is a board-certified veterinary
pathologist. Imaging was performed using a DM5500 micro-
scope, and LAS software was used for image acquisition (Leica).

Long-term imaging of adult tumor–bearing zebrafish using intubation

Time-lapse videos were generated from tumor-bearing ze-
brafish by first anesthetizing fish in 0.17 mg/ml tricaine.
Anesthetized fish were placed on nontoxic modeling clay, and
Tygon tubing was placed over the fish between the caudal fin
and the body to minimize movement. The anesthetized animal
was fully submerged in a water bath containing 0.17 mg/ml
tricaine, and a p200 pipette tip was placed at the edge of the
animal's mouth to provide a steady stream of 0.17 mg/ml
tricaine in tank water through the mouth and over the gills
of the fish. This was accomplished by connecting a peristal-
tic pump to a pipette tip, which delivered oxygenated water
with 0.17 mg/ml tricaine at a rate of 750 μl/min. Cells were
imaged with a 20× water-dipping lens on a DM5500 micro-
scope (Leica). Once the imaging experiment was completed,

Zebrafish T reg–like cells | Kasheta et al.

the fish was revived by pumping fresh water through the pipette tip into the mouth until motion in the gills was evident. After intubation, the Tygon tubing and pipette tip were removed, and the animal was placed back into fresh water for recovery. Image acquisition, background subtraction, and deconvolution were performed with Leica LAS software.

Statistical analysis

Statistical analyses were performed using Prism software by GraphPad. Unless otherwise specified, comparisons between sample groups were performed using unpaired t tests. Comparisons between survival curves were performed by log–rank (Mantel–Cox) tests. Statistical analyses of single-cell profiling data were performed as previously described (Moore et al., 2016a).

Online supplemental material

Fig. S1 shows flow cytometry profiles of *foxp3a:EGFP* –positive cells in WKM and skin, quantification of gene expression in *foxp3a:EGFP*-positive cells from skin, and imaging of *foxp3a:EGFP*-positive cells in skin and muscle. Fig. S2 shows quantification of gene expression in and single–cell profiling of *foxp3a:EGFP*-positive lymphocytes from WKM. Fig. S3 shows characterization of *foxp3a* mutants, including expansion of *Tg(foxp3a:EGFP)*-expressing lymphocytes, quantification of gene expression, small stature, expansion of splenic size and splenic lymphocytes, and quantification of *tnfa* in colon and skin lymphocytes. Video 1 shows live imaging of motile *foxp3a:EGFP*-positive cells in skin.

REFERENCES

Ali, N., B. Zirak, R.S. Rodriguez, M.L. Pauli, H.A. Truong, K. Lai, R. Ahn, K. Corbin, M.M. Lowe, T.C. Scharschmidt, et al. 2017. Regulatory T cells in skin facilitate epithelial stem cell differentiation. *Cell.* 169:1119–1129. https://doi.org/10.1016/j.cell.2017.05.002

Andersen, K.G., J.K. Nissen, and A.G. Betz. 2012. Comparative genomics reveals key gain-of-function events in Foxp3 during regulatory T cell evolution. *Front. Immunol.* 3:113. https://doi.org/10.3389/fimmu.2012.00113

Anelli, V., J.A. Villefranc, S. Chhangawala, R. Martinez-McFaline, E. Riva, A. Nguyen, A. Verma, R. Bareja, Z. Chen, T. Scognamiglio, et al. 2017. Oncogenic BRAF disrupts thyroid morphogenesis and function via twist expression. *eLife.* 6:e20728. https://doi.org/10.7554/eLife.20728

Bauer, C.A., E.Y. Kim, F. Marangoni, E. Carrizosa, N.M. Claudio, and T.R. Mempel. 2014. Dynamic Treg interactions with intratumoral APCs promote local CTL dysfunction. *J. Clin. Invest.* 124:2425–2440. https://doi.org/10.1172/JCI66375

Bennett, C.L., J. Christie, F. Ramsdell, M.E. Brunkow, P.J. Ferguson, L. Whitesell, T.E. Kelly, F.T. Saulsbury, P.F. Chance, and H.D. Ochs. 2001. The immune dysregulation, polyendocrinopathy, enteropathy, X-linked syndrome (IPEX) is caused by mutations of FOXP3. *Nat. Genet.* 27:20–21. https://doi.org/10.1038/83713

Birzele, F., T. Fauti, H. Stahl, M.C. Lenter, E. Simon, D. Knebel, A. Weith, T. Hildebrandt, and D. Mennerich. 2011. Next-generation insights into regulatory T cells: Expression profiling and FoxP3 occupancy in human. *Nucleic Acids Res.* 39:7946–7960. https://doi.org/10.1093/nar/gkr444

Brunkow, M.E., E.W. Jeffery, K.A. Hjerrild, B. Paeper, L.B. Clark, S.A. Yasayko, J.E. Wilkinson, D. Galas, S.F. Ziegler, and F. Ramsdell. 2001. Disruption of a new forkhead/winged-helix protein, scurfin, results in the fatal lymphoproliferative disorder of the scurfy mouse. *Nat. Genet.* 27:68–73. https://doi.org/10.1038/83784

Dee, C.T., R.T. Nagaraju, E.I. Athanasiadis, C. Gray, L. Fernandez Del Ama, S.A. Johnston, C.J. Secombes, A. Cvejic, and A.F. Hurlstone. 2016. CD4-transgenic zebrafish reveal tissue-resident Th2- and regulatory T cell-like populations and diverse mononuclear phagocytes. *J. Immunol.* 197:3520–3530. https://doi.org/10.4049/jimmunol.1600959

Dobin, A., C.A. Davis, F. Schlesinger, J. Drenkow, C. Zaleski, S. Jha, P. Batut, M. Chaisson, and T.R. Gingeras. 2013. STAR: Ultrafast universal RNA-seq aligner. *Bioinformatics.* 29:15–21. https://doi.org/10.1093/bioinformatics/bts635

Flajnik, M.F., and M. Kasahara. 2010. Origin and evolution of the adaptive immune system: Genetic events and selective pressures. *Nat. Rev. Genet.* 11:47–59. https://doi.org/10.1038/nrg2703

Frazer, J.K., N.D. Meeker, L. Rudner, D.F. Bradley, A.C. Smith, B. Demarest, D. Joshi, E.E. Locke, S.A. Hutchinson, S. Tripp, et al. 2009. Heritable T-cell malignancy models established in a zebrafish phenotypic screen. *Leukemia.* 23:1825–1835. https://doi.org/10.1038/leu.2009.116

Gavin, M.A., T.R. Torgerson, E. Houston, P. DeRoos, W.Y. Ho, A. Stray-Pedersen, E.L. Ocheltree, P.D. Greenberg, H.D. Ochs, and A.Y. Rudensky. 2006. Single-cell analysis of normal and FOXP3-mutant human T cells: FOXP3 expression without regulatory T cell development. *Proc. Natl. Acad. Sci. USA.* 103:6659–6664. https://doi.org/10.1073/pnas.0509484103

Hill, J.A., M. Feuerer, K. Tash, S. Haxhinasto, J. Perez, R. Melamed, D. Mathis, and C. Benoist. 2007. Foxp3 transcription-factor-dependent and –independent regulation of the regulatory T cell transcriptional signature. *Immunity.* 27:786–800. https://doi.org/10.1016/j.immuni.2007.09.010

Hillhouse, E.E., and S. Lesage. 2013. A comprehensive review of the phenotype and function of antigen-specific immunoregulatory double negative T cells. *J. Autoimmun.* 40:58–65. https://doi.org/10.1016/j.jaut.2012.07.010

Howe, K., M.D. Clark, C.F. Torroja, J. Torrance, C. Berthelot, M. Muffato, J.E. Collins, S. Humphray, K. McLaren, L. Matthews, et al. 2013. The zebrafish reference genome sequence and its relationship to the human genome. *Nature.* 496:498–503. https://doi.org/10.1038/nature12111

Josefowicz, S.Z., L.F. Lu, and A.Y. Rudensky. 2012. Regulatory T cells: Mechanisms of differentiation and function. *Annu. Rev. Immunol.* 30:531–564. https://doi.org/10.1146/annurev.immunol.25.022106.141623

Kim, J.M., J.P. Rasmussen, and A.Y. Rudensky. 2007. Regulatory T cells prevent catastrophic autoimmunity throughout the lifespan of mice. *Nat. Immunol.* 8:191–197. https://doi.org/10.1038/ni1428

Kwan, K.M., E. Fujimoto, C. Grabher, B.D. Mangum, M.E. Hardy, D.S. Campbell, J.M. Parant, H.J. Yost, J.P. Kanki, and C.B. Chien. 2007. The Tol2kit: A multisite gateway-based construction kit for Tol2 transposon transgenesis constructs. *Dev. Dyn.* 236:3088–3099. https://doi.org/10.1002/dvdy.21343

Lahl, K., C. Loddenkemper, C. Drouin, J. Freyer, J. Arnason, G. Eberl, A. Hamann, H. Wagner, J. Huehn, and T. Sparwasser. 2007. Selective depletion of Foxp3$^+$ regulatory T cells induces a scurfy-like disease. *J. Exp. Med.* 204:57–63. https://doi.org/10.1084/jem.20061852

Langenau, D.M., A.A. Ferrando, D. Traver, J.L. Kutok, J.P. Hezel, J.P. Kanki, L.I. Zon, A.T. Look, and N.S. Trede. 2004. In vivo tracking of T cell development, ablation, and engraftment in transgenic zebrafish. *Proc. Natl. Acad. Sci. USA.* 101:7369–7374. https://doi.org/10.1073/pnas.0402248101

Lin, H.F., D. Traver, H. Zhu, K. Dooley, B.H. Paw, L.I. Zon, and R.I. Handin. 2005. Analysis of thrombocyte development in CD41-GFP transgenic zebrafish. *Blood.* 106:3803–3810. https://doi.org/10.1182/blood-2005-01-0179

Lin, W., D. Haribhai, L.M. Relland, N. Truong, M.R. Carlson, C.B. Williams, and T.A. Chatila. 2007. Regulatory T cell development in the absence of functional Foxp3. *Nat. Immunol.* 8:359–368. https://doi.org/10.1038/ni1445

Liu, Z., M.Y. Gerner, N. Van Panhuys, A.G. Levine, A.Y. Rudensky, and R.N. Germain. 2015. Immune homeostasis enforced by co-localized effector and regulatory T cells. *Nature.* 528:225–230. https://doi.org/10.1038/nature16169

Love, M.I., W. Huber, and S. Anders. 2014. Moderated estimation of fold change and dispersion for RNA-seq data with DESeq2. *Genome Biol.* 15:550. https://doi.org/10.1186/s13059-014-0550-8

Lyon, M.F., J. Peters, P.H. Glenister, S. Ball, and E. Wright. 1990. The scurfy mouse mutant has previously unrecognized hematological abnormalities and resembles Wiskott-Aldrich syndrome. *Proc. Natl. Acad. Sci. USA.* 87:2433–2437. https://doi.org/10.1073/pnas.87.7.2433

Marson, A., K. Kretschmer, G.M. Frampton, E.S. Jacobsen, J.K. Polansky, K.D. MacIsaac, S.S. Levine, E. Fraenkel, H. von Boehmer, and R.A. Young. 2007. Foxp3 occupancy and regulation of key target genes during T-cell stimulation. *Nature.* 445:931–935. https://doi.org/10.1038/nature05478

Mempel, T.R., M.J. Pittet, K. Khazaie, W. Weninger, R. Weissleder, H. von Boehmer, and U.H. von Andrian. 2006. Regulatory T cells reversibly suppress cytotoxic T cell function independent of effector differentiation. *Immunity.* 25:129–141. https://doi.org/10.1016/j.immuni.2006.04.015

Moore, F.E., E.G. Garcia, R. Lobbardi, E. Jain, Q. Tang, J.C. Moore, M. Cortes, A. Molodtsov, M. Kasheta, C.C. Luo, et al. 2016a. Single-cell transcriptional analysis of normal, aberrant, and malignant hematopoiesis in zebrafish. *J. Exp. Med.* 213:979–992. https://doi.org/10.1084/jem.20152013

Moore, J.C., Q. Tang, N.T. Yordán, F.E. Moore, E.G. Garcia, R. Lobbardi, A. Ramakrishnan, D.L. Marvin, A. Anselmo, R.I. Sadreyev, and D.M. Langenau. 2016b. Single-cell imaging of normal and malignant cell engraftment into optically clear prkdc-null SCID zebrafish. *J. Exp. Med.* 213:2575–2589. https://doi.org/10.1084/jem.20160378

Panduro, M., C. Benoist, and D. Mathis. 2016. Tissue Tregs. *Annu. Rev. Immunol.* 34:609–633. https://doi.org/10.1146/annurev-immunol-032712-095948

Powell, B.R., N.R. Buist, and P. Stenzel. 1982. An X-linked syndrome of diarrhea, polyendocrinopathy, and fatal infection in infancy. *J. Pediatr.* 100:731–737. https://doi.org/10.1016/S0022-3476(82)80573-8

Robertson, A.L., S. Avagyan, J.M. Gansner, and L.I. Zon. 2016. Understanding the regulation of vertebrate hematopoiesis and blood disorders—Big lessons from a small fish. *FEBS Lett.* 590:4016–4033. https://doi.org/10.1002/1873-3468.12415

Roychoudhuri, R., R.L. Eil, and N.P. Restifo. 2015. The interplay of effector and regulatory T cells in cancer. *Curr. Opin. Immunol.* 33:101–111. https://doi.org/10.1016/j.coi.2015.02.003

Subramanian, A., P. Tamayo, V.K. Mootha, S. Mukherjee, B.L. Ebert, M.A. Gillette, A. Paulovich, S.L. Pomeroy, T.R. Golub, E.S. Lander, and J.P. Mesirov. 2005. Gene set enrichment analysis: A knowledge-based approach for interpreting genome-wide expression profiles. *Proc. Natl. Acad. Sci. USA.* 102:15545–15550. https://doi.org/10.1073/pnas.0506580102

Sugimoto, N., T. Oida, K. Hirota, K. Nakamura, T. Nomura, T. Uchiyama, and S. Sakaguchi. 2006. Foxp3-dependent and -independent molecules specific for CD25+CD4+ natural regulatory T cells revealed by DNA microarray analysis. *Int. Immunol.* 18:1197–1209. https://doi.org/10.1093/intimm/dxl060

Traver, D., B.H. Paw, K.D. Poss, W.T. Penberthy, S. Lin, and L.I. Zon. 2003. Transplantation and in vivo imaging of multilineage engraftment in zebrafish bloodless mutants. *Nat. Immunol.* 4:1238–1246. https://doi.org/10.1038/ni1007

Wen, Y., W. Fang, L.X. Xiang, R.L. Pan, and J.Z. Shao. 2011. Identification of Treg-like cells in Tetraodon: Insight into the origin of regulatory T subsets during early vertebrate evolution. *Cell. Mol. Life Sci.* 68:2615–2626. https://doi.org/10.1007/s00018-010-0574-5

Wienholds, E., S. Schulte-Merker, B. Walderich, and R.H. Plasterk. 2002. Target-selected inactivation of the zebrafish rag1 gene. *Science.* 297:99–102. https://doi.org/10.1126/science.1071762

Wildin, R.S., F. Ramsdell, J. Peake, F. Faravelli, J.L. Casanova, N. Buist, E. Levy-Lahad, M. Mazzella, O. Goulet, L. Perroni, et al. 2001. X-linked neonatal diabetes mellitus, enteropathy and endocrinopathy syndrome is the human equivalent of mouse scurfy. *Nat. Genet.* 27:18–20. https://doi.org/10.1038/83707

Wildin, R.S., S. Smyk-Pearson, and A.H. Filipovich. 2002. Clinical and molecular features of the immunodysregulation, polyendocrinopathy, enteropathy, X linked (IPEX) syndrome. *J. Med. Genet.* 39:537–545. https://doi.org/10.1136/jmg.39.8.537

Yoon, S., S. Mitra, C. Wyse, A. Alnabulsi, J. Zou, E.M. Weerdenburg, A.M. van der Sar, D. Wang, C.J. Secombes, and S. Bird. 2015. First demonstration of antigen induced cytokine expression by CD4-1$^+$ lymphocytes in a poikilotherm: Studies in zebrafish (*Danio rerio*). *PLoS One.* 10:e0126378. https://doi.org/10.1371/journal.pone.0126378

Zheng, Y., S.Z. Josefowicz, A. Kas, T.T. Chu, M.A. Gavin, and A.Y. Rudensky. 2007. Genome-wide analysis of Foxp3 target genes in developing and mature regulatory T cells. *Nature.* 445:936–940. https://doi.org/10.1038/nature05563